Feasibility of a finite-difference time-domain model in large-scale acoustic simulations

The Journal of the Acoustical Society of America

Feasibility of a finite-difference time-domain model in large-scale acoustic simulations

--Manuscript Draft--

Manuscript Number:	JASA-07354R3
Full Title:	Feasibility of a finite-difference time-domain model in large-scale acoustic simulations
Article Type:	Regular Article
Corresponding Author:	Dario D'Orazio, Ph.D. University of Bologna Bologna, ITALY
First Author:	Giulia Fratoni, Ph.D.
Order of Authors:	Giulia Fratoni, Ph.D.
	Brian Hamilton
	Dario D'Orazio
Section/Category:	Architectural Acoustics
Keywords:	finite-difference time-domain simulations; Architectural acoustics; wave-based techniques; opera houses; multi-decay analysis.
Abstract:	Wave-based techniques for room acoustics simulations are commonly applied to low frequency analysis and small-sized simplified environments. The constraints are generally the inherent computational cost and the challenging implementation of proper complex boundary conditions. Nevertheless, the application field of wave-based simulation methods has been extended in the latest research decades. With the aim of testing this potential, the present work investigates the feasibility of a Finite-Difference Time-Domain (FDTD) code simulating large non-trivial geometries in wide frequency ranges. A representative sample of large coupled-volume opera houses allowed demonstration of the capability of the selected FDTD model to tackle such composite geometries up to 4 kHz. For such a demanding task, efficient calculation schemes and frequency-dependent boundary admittances are implemented in the simulation framework. The results of in situ acoustic measurements were used as benchmark during the calibration process of 3D virtual models. In parallel, acoustic simulations performed on the same halls through standard ray-tracing techniques enabled a systematic comparison between the two numerical approaches highlighting significant differences in terms of input data. The ability of the FDTD code to detect the typical acoustic scenarios occurring in coupled-volume halls is confirmed through multi-slope decay analysis and impulse responses' spectral content.
Additional Information:	
Question	**Response**
Please read the Transfer of Copyright Agreement and the Instructions. By selecting the appropriate response below, you verify that you have consented to the Transfer of Copyright Agreement (if applicable) and the conditions and representations set forth in the Instructions.	R - Regular

Feasibility of a finite-difference time-domain model in large-scale acoustic simulations

Giulia Fratoni,[1] Brian Hamilton,[2] and Dario D'Orazio[1]

[1]*Department of Industrial Engineering, University of Bologna, Bologna, 40136, Italy*

[2]*Acoustics and Audio Group, University of Edinburgh, Edinburgh, UK*

Wave-based techniques for room acoustics simulations are commonly applied to low frequency analysis and small-sized simplified environments. The constraints are generally the inherent computational cost and the challenging implementation of proper complex boundary conditions. Nevertheless, the application field of wave-based simulation methods has been extended in the latest research decades. With the aim of testing this potential, the present work investigates the feasibility of a Finite-Difference Time-Domain (FDTD) code simulating large non-trivial geometries in wide frequency ranges. A representative sample of large coupled-volume opera houses allowed demonstration of the capability of the selected FDTD model to tackle such composite geometries up to 4 kHz. For such a demanding task, efficient calculation schemes and frequency-dependent boundary admittances are implemented in the simulation framework. The results of *in situ* acoustic measurements were used as benchmark during the calibration process of 3D virtual models. In parallel, acoustic simulations performed on the same halls through standard ray-tracing techniques enabled a systematic comparison between the two numerical approaches highlighting significant differences in terms of input data. The ability of the FDTD code to detect the typical acoustic scenarios occurring in coupled-volume halls is confirmed through multi-slope decay analysis and impulse responses' spectral content.

I. INTRODUCTION

Room acoustics simulation methods are traditionally classified in two distinct groups: the first one based on the description of sound propagation through the wave equation, the second one based on the approximation through rays (Savioja and Svensson, 2015; Vorländer, 2020). The wave-based approach approximates the resolution of the wave equation by employing spatial (Marburg and Nolte, 2008) or spatiotemporal discretization (Botteldooren, 1995; Pind *et al.*, 2019) of the system domains. The outcomes of this category remain physically and theoretically valid in the whole frequency range, at the expense of high computational cost and a certain degree of numerical dispersion (Bilbao, 2009). For this reason, the application field is usually limited to low-medium frequencies and small rooms (Soares *et al.*, 2022). The ray-based approach, commonly defined as Geometrical Acoustics (GA), finds its roots in computer graphics principles, i.e. the assumption that sound propagates through rays (Krokstad *et al.*, 1968). It is widely accepted in literature that the GA approach is sufficiently accurate above the Schroeder frequency and when the dimensions of the hall are large enough compared to the wavelengths (Bork, 2005). Even though great effort has been made to compensate the respective weaknesses of the two macro-categories of simulation methods (Jeong *et al.*, 2008; Marbjerg *et al.*, 2015; Wareing and Hodgson, 2005), scholars generally agree with the use of hybrid models, that are expected to provide accurate broadband results exploiting the benefits and minimizing the drawbacks of each approach (Jeong, 2012; Savioja, 2010; Southern *et al.*, 2013).

The present study employs a set of large non-trivial geometries to investigate the performance of a Finite-Difference Time-Domain (FDTD) model combined with a classical GA algorithm. Four coupled-volume large halls (from 9000 m^3 to 25000 m^3) were selected as a significant test sample to thoroughly explore the feasibility of the FDTD model in this uncommon application field. As assessed in previous studies (Luizard *et al.*, 2013; Wang *et al.*, 2019), the accuracy of the results is explored through Bayesian multi-decay analysis (Xiang *et al.*, 2011) and frequency responses for particular source-receiver pairs (Lai and Hamilton, 2020; Soares *et al.*, 2022). During the present work, the impulse responses acquired through in-situ measurements were used as a reference point while the same 3D virtual models calibrated with standard GA techniques were considered by way of comparison. With a special focus on the input data involved (Jeong, 2009; Mondet *et al.*, 2020), the present work also aims to enlarge the benchmark in computational acoustics with further datasets (Hornikx *et al.*, 2015b).

This paper is organised as follows. A brief description of FDTD methods and their main features is reported in Section II. In Section III the overall workflow is illustrated: the case studies, the measurements, GA and FDTD simulations' setup. Section IV presents the different input data employed in FDTD and GA calibration processes. Finally, results of specific investigations on the FDTD code's accuracy to detect challenging acoustic scenarios are provided in Section V.

II. FINITE-DIFFERENCE TIME-DOMAIN METHODS

The acoustic field within an enclosure can be described in terms of the scalar field velocity potential $u = u(\mathbf{x}, t)$ through the partial differential equation (PDE):

$$\Big(\nabla^2 - \frac{1}{c^2}\frac{\partial^2}{\partial t^2}\Big)u = 0 \tag{1}$$

where ∇^2 is the 3D Laplacian operator, c is the sound speed in air, assumed as 343 m/s at $\mathrm{T} = 20°C$ and relative humidity (RH) at $= 50\%$. The relation between the velocity potential $u = u(\mathbf{x}, t)$, the sound pressure $p = p(\mathbf{x}, t)$, and the vector particle velocity $\mathbf{v}$ is expressed by the equations:

$$p = -\rho\frac{\partial u}{\partial t}, \qquad \mathbf{v} = -\nabla u \tag{2}$$

where ρ is the density of air, assumed as $1.213\,\mathrm{kg/m^3}$ at $\mathrm{T} = 20°C$ and $\mathrm{RH} = 50\%$. Given the impossibility of finding the exact analytical solution of Equation 1 in large non-trivial geometries, a common feature of all the wave-based methods is the replacement of continuous domains with spatial or spatiotemporal discrete grids.

The FDTD methods - which are among the oldest methods to solve PDEs (Courant *et al.*, 1928) - approximate the spatial and the temporal derivatives of the differential equations, calculating the numerical solution as a temporal recursion over a space grid (Botteldooren, 1995). The solution $u(\mathbf{x}, t)$ of the wave equation, with $\mathbf{x} \in \mathbb{R}^3$, may be approximated by a grid function $u^n_{l,m,p}$ where

$$x = lh \qquad y = mh, \qquad z = ph, \qquad t = nk \tag{3}$$

being l, m, n, p integer numbers, h the grid spacing, and k the time step. A group of explicit FDTD methods follows the same general scheme (Kowalczyk and Van Walstijn, 2010):

$$\delta_t^2 u_{l,m,p}^n = \lambda^2[(\delta_x^2 + \delta_y^2 + \delta_z^2) + a(\delta_x^2\delta_y^2 + \delta_x^2\delta_z^2 + \delta_y^2\delta_z^2) + b(\delta_x^2\delta_y^2\delta_z^2)]u_{l,m,p} \tag{4}$$

where λ is the dimensionless quantity defined as the Courant number $\lambda = ck/h$ and a and b are specific coefficients of each scheme. For instance, the choice of $a = b = 0$ provides the simplest Cartesian scheme, which is updated at each point $u_{l,m,p}^{n+1}$ with the equation:

$$u_{l,m,p}^{n+1} = (2 - 6\lambda^2)u_{l,m,p}^n + \lambda^2 S_{l,m,p} - u_{l,m,p}^{n-1} \tag{5}$$

where $S_{l,m,p} = u_{l+1,m,p}^n + u_{l-1,m,p}^n + u_{l,m+1,p}^n + u_{l,m-1,p}^n + u_{l,m,p+1}^n + u_{l,m,p-1}^n$ is a sum over nearest neighbours on the Cartesian grid. The fact that the update recursion is parallelisable over the spatial grid permits the use of parallel computing architectures, such as GPUs or multi-core CPUs (Webb and Bilbao, 2011).

A. Choosing grid spacing and time-step

Given the number of points per wavelength (PPW) corresponding to the desired dispersion error (1%–2% in the present study (Hamilton, 2016)), the lower the h value, the higher the upper frequency f_{max} simulated by the FDTD model according to the expression (Bilbao, 2009):

$$h = \frac{c}{\mathrm{PPW} f_{max}}. \tag{6}$$

As a first approximation the computational cost is proportional to h^{-3}, and thus to f^3 per time step, leading to much more simulation time required for small values of grid spacing

and for higher frequencies (Hamilton, 2016). Once h is set, the time-step is set according to stability considerations. A scheme is defined as *stable* when the solutions of the system do not grow exponentially and the Fourier transform uniformly converges (Strikwerda, 1989). The stability condition primarily depends on the Courant number λ, which is limited to:

$$\lambda \leq \left(\max\left[1, 2-4a, 3-12a+16b\right]\right)^{-1/2} \tag{7}$$

which is the so-called Courant-Friedrichs-Lewy (CLF) condition (Courant *et al.*, 1928) for this family of schemes. The consequent maximum value of time step in a 3D system is $k \leq \lambda h/c$, and generally the limit of stability is chosen for efficiency reasons.

B. Boundary conditions

Locally-reactive complex-admittances $Y(\mathbf{x}, s)$ are employed as boundary conditions. The general expression of the relation between the pressure $p(\mathbf{x}, s)$ and the normal velocity component at the boundary $\mathbf{n} \cdot \mathbf{v}(\mathbf{x}, s)$ is:

$$Y(\mathbf{x}, s)p(\mathbf{x}, s) = \mathbf{n} \cdot \mathbf{v}(\mathbf{x}, s) \tag{8}$$

where s is the usual transform variable (Bilbao *et al.*, 2015). The electrical-acoustical analogy with a parallel network of LRC circuits is employed as a one-port structure:

$$Y(\mathbf{x}, s) = \sum_{m=1}^{M} \frac{s}{L^{(m)}(\mathbf{x})s^2 + R^{(m)}(\mathbf{x})s + \frac{1}{C^{(m)}(\mathbf{x})}} \tag{9}$$

where $Y(\mathbf{x}, s)$ is the complex admittance, L, R, C are, respectively, the real-valued non-negative inductance, resistance and capacitance of the circuit, M is the number of different branches involved in the circuit.

III. METHOD

A. Case studies

Since the aim of the present work is to test the potential of a FDTD model in applications commonly considered as disadvantageous for wave-based methods, four large-scale opera houses have been selected as case studies. The significant size associated with those composite architectures is already a demanding task and time consuming for any 3D wave-based approach (Webb and Bilbao, 2011). A further challenge is the variety of acoustic characteristics throughout the audience areas, which is typical of such coupled-volume halls. Moreover, the fact that the volumetric proportions are completely different in the opera houses under study allows the analysis of the particular traits of each subcategory of halls (Hidaka and Beranek, 2000; Prodi *et al.*, 2015). A schematic geometrical representation of

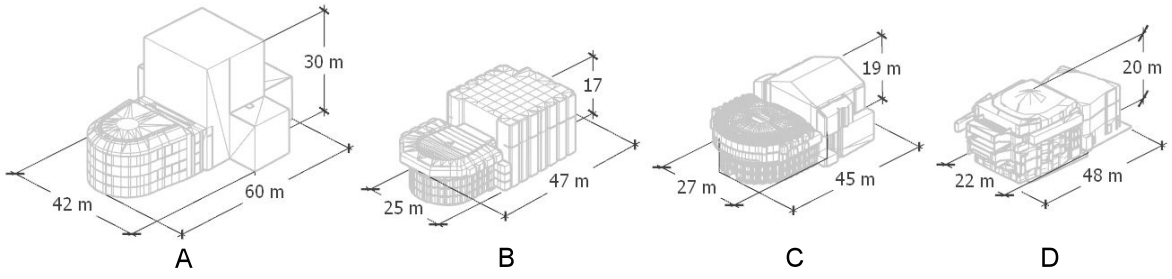

FIG. 1. (Color online) Geometrical representation and main dimensions of the coupled-volume halls under study.

the halls is provided in Figure 1 along with their main dimensions.

The first two halls show a relevant disproportion between the volume of the stage tower and the rest of the theatre affecting the sound energy decays at the listeners with significant

TABLE I. Details of the coupled-volume halls under study. Total volume (V), the main hall volume (V_{hall}), the maximum seating capacity (N), the reverberation time value averaged over 500 - 1000 Hz ($T_{30,M}$), the Schroeder frequency (f_c), the number of sound source (S) and receiver (R) locations, and the coupling factor (k_c) are provided for each hall.

Hall ID	V (m^3)	V_{hall} (m^3)	N	$T_{30,M}$ (s)	f_c (Hz)	S	R	k_c
A	25400	5400	1030	1.53	16	4	25	0.35
B	12030	3000	800	1.77	24	2	23	0.25
C	10450	4000	835	1.37	23	2	23	0.13
D	8640	7400	1000	1.32	25	3	18	0.18

coupling effects (Garai *et al.*, 2016, 2015). The unusual large-sized fly-tower combined with limited absorbing materials, such as draperies or opera sceneries, contribute to place hall A and hall B in the first category of a specific taxonomy of performance spaces developed for international opera houses by (Hidaka and Beranek, 2000) and adapted for Italian opera houses by (Prodi *et al.*, 2015). Instead, the third hall shows regular proportions between the stage house and the main hall, along with highly absorbing materials in the former volume. These features contribute to rank hall C in the second category of the aforementioned taxonomy. The fourth space, hall D, belongs to the "modern" category (Prodi *et al.*, 2015) due the specific design of the early reflection paths exploiting large balconies instead of single boxes (D'Orazio *et al.*, 2020a). The main details about the coupled-volume halls

are provided in Table I: the total volume (V), the main hall volume (V_{hall}), the maximum seating capacity (N), the reverberation time value averaged over 500 - 1000 Hz ($T_{30,M}$), the Schroeder frequency (f_c), the number of sound source (S) and receiver (R) locations, and the coupling factor (k_c). With reference to the classical coupled volumes thoery (Cremer and Müller, 1978), this last parameter refers to the sound source in the fly tower and the receiver in the main hall.

B. Measurements

The four performance spaces have been acoustically assessed by means of several measurement campaigns allowing the collection of a considerable amount of reference data in terms of acquired impulse responses and objective room criteria (Garai *et al.*, 2016). During the acoustic surveys the opera houses were in unoccupied conditions in compliance with the reference standard ISO 3382-1. Each stage house was equipped with the usual opera scenery and sound absorbing objects, i.e. drapes and curtains, while each orchestra pit was lacking chairs and music stands. The impulse responses for each sound source-receiver pair were acquired using a 5 second exponential sine sweep (ESS) signal. A custom high-SPL dodecahedron was adopted as an omnidirectional source (D'Orazio *et al.*, 2016) and four Brüel & Kjær 4190 microphones were employed as monoaural receivers. The locations of sound sources and receivers were chosen following the Ferrara Charter procedure (Pompoli and Prodi, 2000). As can be seen in Figure 2, at least two sound source locations were chosen in each hall: the first below the proscenium arch and the second at the centre of the stage. Where possible, two extra points for the sound source were considerd in the orchestra pit, in

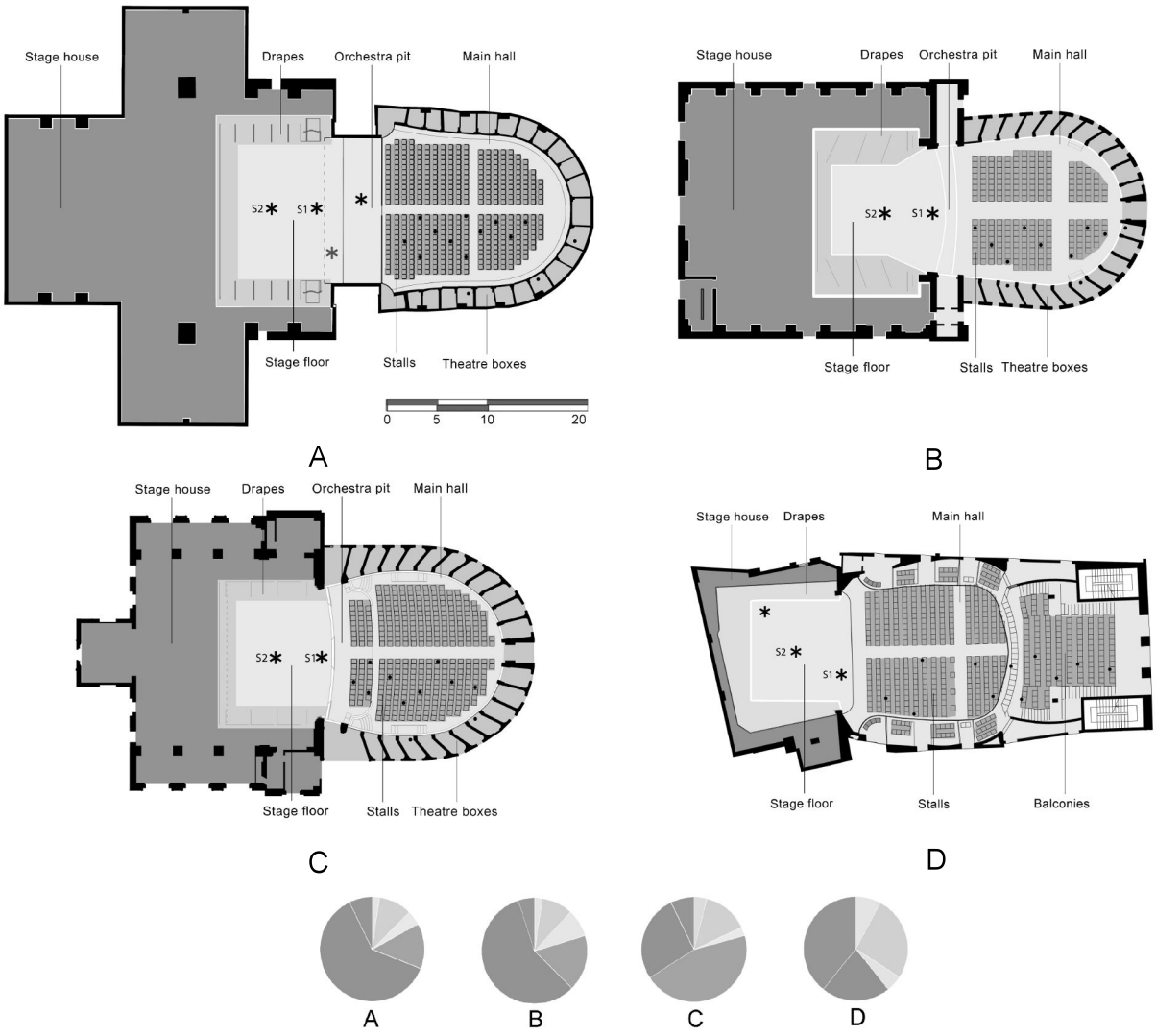

FIG. 2. (Color online) Sound source (*) and receiver (•) measurement plans of the surveyed coupled-volume halls. Pie charts show the proportion of materials labelled in the plans in terms of equivalent absorption area percentage, $\%A_{eq}$ (mean values are taken over 500 Hz and 1000 Hz.)

the covered and uncovered parts (see A in Figure 2). Receivers were organized following a dense mesh of points in one half of the audience areas, exploiting the symmetry of the main hall. A large number of receiver points were employed during the measurements to better detect the various acoustic characteristics in stalls, boxes, galleries (or balconies in D) (Sato

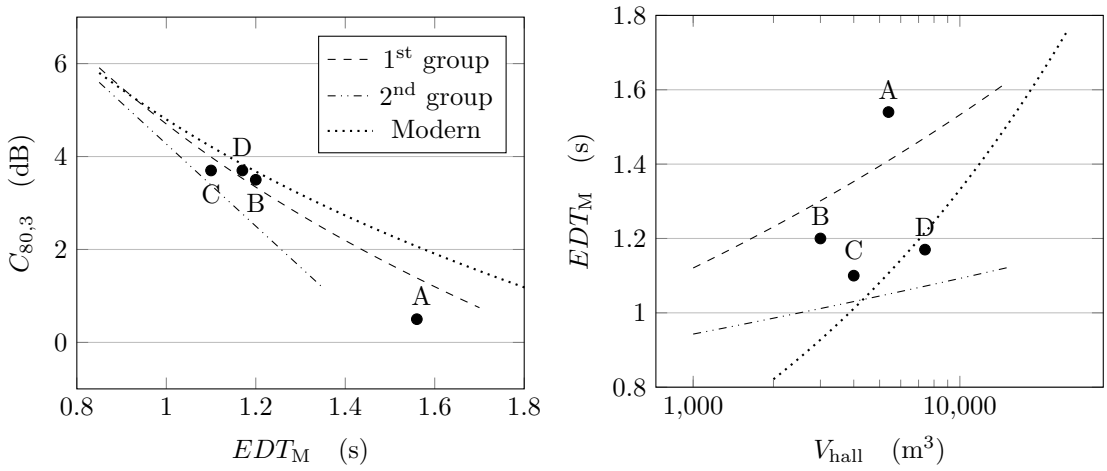

FIG. 3. Measured values of $C_{80,3}$ vs EDT_M (left) and EDT_M vs V_{hall} (right) of the coupled-volume halls under study. $C_{80,3}$ values are averaged over 500 Hz - 1000 Hz - 2000 Hz and EDT_M over 500 Hz - 1000 Hz. The three categories correspond to the taxonomy provided by (Hidaka and Beranek, 2000) for international opera houses and readapted by (Prodi *et al.*, 2015) for Italian opera houses with the additional "modern" category.

et al., 2012). Also, in Figure 2 the main materials have been labelled and identified through different colours. Pie charts at the bottom of the same figure point out the different acoustic category of the halls according to the distribution of the materials' equivalent absorption area, $\%\mathrm{A}_{\mathrm{eq}}$, whose values have been averaged over 500 Hz and 1000 Hz. Moreover, measured relationships between C_{80} vs EDT_{M}, and EDT_{M} vs V_{hall} confirm the aforementioned ranking of the halls, as can be seen in Figure 3 (Prodi *et al.*, 2015).

C. GA simulation

The GA simulation of the opera houses has been carried out with the hybrid ray-based commercial software Odeon Room Acoustics and according to the state-of-art procedure

(Brinkmann *et al.*, 2019; Vorländer, 2020). The 3D virtual models were built with the proper geometry reduction required in room acoustics (Siltanen *et al.*, 2008) using Trimble SketchUp. The transition order (TO) as defined in the Odeon system parameters is the order of reflection threshold determining a switch between the use of the image source method and stochastic ray-tracing for predicting an impulse response. It was set equal to 0, as recommended for non-trivial geometries with a large number of surfaces (Christensen, 1998; Rindel, 2000). The number of *late rays* was set equal to 100,000 and the maximum reflection order was chosen equal to 2000 to obtain the highest level of accuracy ("Precision" setup). Temperature and relative humidity were set equal to 20 C° and 50 % in all the GA simulations of the present work, as these were the mean thermo-hygrometric conditions measured *in situ* during the measurements.

During the modeling process the actual number of materials has been reduced to a smaller group of CAD layers to limit the uncertainty of input data, i.e. the acoustic properties assigned to each surface (Vorländer, 2013). This has been obtained by merging materials with similar acoustic features into equivalent macro-layers, as in the case of the "boxes" and "stage house" materials (D'Orazio *et al.*, 2020b, 2019). T_{30}, EDT, C_{80}, T_S have been used as calibration metrics and, respectively, 10%, 10%, 1 dB, 10 ms have been considered as tolerance ranges between measured and simulated values. The numerical models were tuned on the measurements' results by evaluating the mean values of each audience area in each octave band from 125 Hz to 4000 Hz. All the virtual models were calibrated through a first assignment of suitable sound absorption and scattering coefficients to the macro-layers (Vorländer, 2020) and the successive iterative adjustments - within reliable ranges - till the

achievement of the calibration (Pilch, 2020). Particular sound absorbing characteristics of some materials, such as the "stage grid" layer in the fly tower, were taken from a previous survey (Garai *et al.*, 2015) and from specific studies (Kim *et al.*, 2010).

D. FDTD simulation

The FDTD scheme employed in the present study has been developed by (Bilbao *et al.*, 2015; Hamilton *et al.*, 2016). The procedure employed to tune the FDTD models keeping a term of comparison with parallel GA calibrations is presented in Figure 4. The authors chose to maintain the same approximation degree of the 3D geometries suggested for ray-tracing techniques to obtain comparable FDTD and GA results.

For higher efficiency in terms of minimizing dispersion errors, the non-Cartesian 13-point stencil cubic close-packed (CCP) scheme with $a = 1/4, b = 0$ and $\lambda = 1$ (see Eq. (4)) was used over a face-centered cubic (FCC) subgrid. Practical test on GPU have proven the 13-point scheme on the FCC grid to be more suited to large-scale room acoustic simulations rather than, for instance, 27-point schemes on a cubic grid, for equal computational densities (Hamilton and Webb, 2013). Concerning the stability requirement, it has been demonstrated that the maximum Courant number allowed by stability condition (see Equation 7) grants an efficient balance between the desired time cost and the minimization of the dispersion error (Hamilton, 2016). The FDTD scheme was applied up to 4 kHz for the wave-based part of simulated impulse responses. For upper frequencies a classical ray tracing at high-density (1e9 rays) was employed, without the inclusion of scattering or diffraction. A value of PPW= 6.75 was chosen as points-per-wavelength returning numerical dispersion errors between 1%

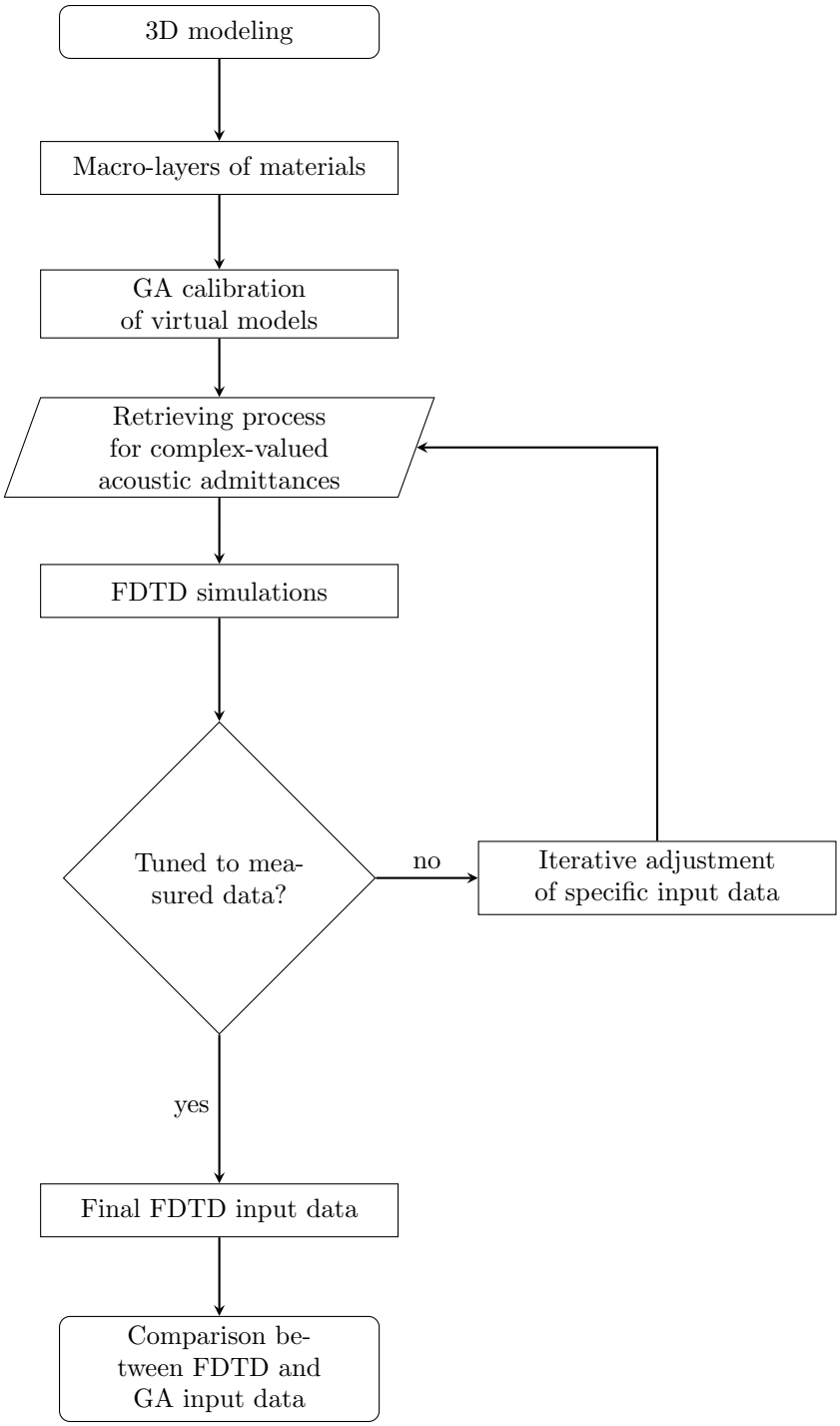

FIG. 4. FDTD calibration process carried out in each of the 3D virtual models, taking the measurements as a reference point and the parallel GA calibration as a term of comparison.

TABLE II. Simulation setup of FDTD simulations. The maximum frequency simulated with FDTD (f_{max}), the points per wavelength (PPW), the oversampling factor (σ), the grid spacing (h), the time step (k), the Courant number (λ), the time cost in terms of hours of runtime per second of computed impulse response (s_{output}), and the dispersion error (in percentage) are provided.

f_{max} (Hz)	PPW	σ	h (mm)	$F_s = 1/k$ (Hz)	λ	Time cost (hours/s_{output})	Dispersion error %
4000	6.75	3.375	12.3	27500	$\simeq 1$	1	1%-2%

and 2%, with a grid spacing equal to $h \simeq 12.3\,\text{mm}$ and a consequent time step equal to $k = 0.03\,\text{ms}$ (see Table II). The impulse response length was set equal to 3 s to include even the higher values of reverberation time at lower frequencies. The computational task has been parallelized using CUDA over four Nvidia Titan X (2015 Maxwell architecture) GPUs, achieving 3 hours per simulated impulse response for each sound source, corresponding to 1 hour per second of simulated impulse response.

Concerning the air absorption, an implementation has been added to the FDTD scheme used in the present work to consider viscothermal effects in air (Hamilton, 2021). In fact, while in small rooms and at low frequencies, that are the usual application fields of wave-based methods, the absorption of the air may be neglected, in large enclosed spaces it should be accurately calculated to obtain reliable simulations (Saarelma and Savioja, 2016). Energy losses caused by the viscosity of air have been introduced into the three-dimensional wave

equation, according to reasonable indoor conditions (relative humidity of the air, temperature and pressure) (Hamilton, 2021).

At the boundaries, the well-known issue of staircase effects in regular-grid FDTD schemes over non-trivial geometries has been overcome through a finite-volume time-domain (FVTD) approach. Fitted cells allowed for a considerable reduction of effective surface area errors (from 50% to even 1%), leading to more accurate estimations of decay times and eventually more consistent simulations (Bilbao *et al.*, 2015).

TABLE III: Summary of FDTD calibrations against measurements: the sound source is placed at the centre of each stage and the receivers are spread throughout the audience areas: stalls, boxes and gallery in A, B, C; stalls and balconies in D. Measured and simulated $T_{30,\mathrm{M}}$, EDT_{M}, $C_{80,\mathrm{M}}$, $T_{\mathrm{S,M}}$, $T_{30,125\,\mathrm{Hz}}$ room criteria are provided along with the corresponding differences. Subscript "M" indicates mean values across the octave bands centered on 500 and 1000 Hz.

Hall Criterion	Receivers											
	Overall			Stalls			Boxes/I balcony			Gallery/II balcony		
	Meas.	Sim.	Diff.	Meas.	Sim.	Diff.	Meas.	Sim.	Diff.	Meas.	Sim.	Diff.
$T_{30,\mathrm{M}}$ (s)	1.57	1.56	0.6%	1.53	1.62	5.5%	1.53	1.56	8.1%	1.66	1.51	9.1%
EDT_{M} (s)	1.54	1.43	7.1%	1.56	1.59	1.7%	1.38	1.33	4.0%	1.69	1.38	18%

A

	$C_{80,\mathrm{M}}$ (dB)	0.1	0.1	0.0	-0.2	-0.2	0.0	1.2	0.3	0.9	-0.8	0.2	1.0
	$T_{\mathrm{S,M}}$ (ms)	119	110	9	122	118	4	106	108	2	130	103	27
	$T_{30,125\,\mathrm{Hz}}$ (s)	1.86	1.92	3.2%	1.82	1.98	8.8%	1.82	1.91	4.9%	1.92	1.87	2.6%
	$T_{30,\mathrm{M}}$ (s)	1.59	1.60	0.6%	1.65	1.68	1.7%	1.61	1.59	1.2%	1.51	1.53	3.1%
	EDT_{M} (s)	1.20	1.27	5.8%	1.25	1.34	7.1%	1.04	1.15	10.7%	1.30	1.31	1.4%
B	$C_{80,\mathrm{M}}$ (dB)	3.5	3.0	0.5	3.4	2.9	0.5	4.3	3.5	0.8	2.7	2.7	0.0
	$T_{\mathrm{S,M}}$ (ms)	75	81	6	75	84	9	70	77	7	79	81	2
	$T_{30,125\,\mathrm{Hz}}$ (s)	2.23	2.26	1.4%	2.29	2.31	0.9%	2.21	2.26	2.3%	2.19	2.20	1.4%
	$T_{30,\mathrm{M}}$ (s)	1.39	1.38	0.7%	1.27	1.34	5.1%	1.22	1.27	4.3%	1.68	1.53	8.8%
	EDT_{M} (s)	1.12	1.17	4.5%	1.15	1.18	2.8%	0.87	1.02	17%	1.35	1.31	2.6%
C	$C_{80,\mathrm{M}}$ (dB)	3.7	3.4	0.3	4.9	4.6	0.3	5.5	4.8	0.8	0.8	0.9	0.1
	$T_{\mathrm{S,M}}$ (ms)	73	78	5	58	65	7	59	69	10	103	99	4
	$T_{30,125\,\mathrm{Hz}}$ (s)	2.07	1.97	4.8%	2.12	2.16	1.9%	1.95	1.80	7.7%	2.15	1.95	9.3%
	$T_{30,\mathrm{M}}$ (s)	1.41	1.44	2.1%	1.40	1.47	4.9%	1.37	1.40	2.3%	1.45	1.45	0.0%
	EDT_{M} (s)	1.17	1.20	2.6%	1.36	1.42	4.1%	1.02	0.97	5.1%	1.13	1.21	6.6%
D	$C_{80,\mathrm{M}}$ (dB)	3.6	3.8	0.2	3.6	3.0	0.6	3.8	4.9	1.1	3.3	3.6	0.3
	$T_{\mathrm{S,M}}$ (ms)	77	76	1	75	83	8	73	64	9	82	81	1

$T_{30,125\,\mathrm{Hz}}$ (s)	1.96	2.05	4.6%	1.95	2.02	3.6%	1.92	2.03	5.7%	2.01	2.09	4.0%

With reference to the process described in Figure 4, FDTD calibration was achieved when simulated room criteria converged to the measured ones in all the octave bands of interest (from 125 Hz to 4000 Hz) considering the sound source at the centre of the stage (Pilch, 2020). Table III summarizes the main calibration results at mid frequencies (500 Hz - 1000 Hz) along with a control index at low frequency ($T_{30,125\,\mathrm{Hz}}$) (Hidaka and Beranek, 2000; Prodi *et al.*, 2015). Measured, simulated and difference values are provided averaged over all the receiver positions and for each listener area: stalls, boxes and gallery in A, B, C; stalls, I balcony, II balcony in D. For C_{80} and T_{S} the Just Noticeable Differences (JNDs) provided by ISO 3382-1 were assumed as the tolerance ranges (Postma and Katz, 2015), whilst for T_{30} and EDT twice the JND value (10% of the measured value) were adopted due to the uncertainty of input data (Vorländer, 2013). At the end of the process, almost all the differences (94%) between simulated and measured values are smaller than the tolerance range chosen for each room criterion. Moreover, even considering 1 JND (5%) also for T_{30} and EDT values, the percentage remains high enough for calibration purposes (85% of the values) (Alvarez-Morales and Martellotta, 2015).

IV. FDTD VS GA DATASETS

The present section concerns the material properties employed as boundary conditions in the two simulation approaches. As already stated in Section III D, the calibration process was carried out on the same 3D virtual models of the halls to allow a comparison between

two distinct results obtained from procedures with a common starting point. However, one of the main issues in comparing such different input data is the way to convert the energy parameters employed in GA simulations into non-unique frequency dependent complex surface impedances (Jeong, 2012; Mondet *et al.*, 2020; Rindel, 2011). In the present work, boundary impedance conditions were derived from the energy parameters employed in GA calibrations using the electrical-acoustical analogy mentioned in Section II B and thoroughly described in (Bilbao *et al.*, 2015).

With reference to Figure 4, the iterative process of input data's adjustment for FDTD calibrations was guided by specific reasons: modifications have been applied to those materials and those octave bands whose α_{GA} are expected to be mostly affected by uncertainties (Jeong *et al.*, 2016; Savioja and Svensson, 2015; Vercammen, 2019). The approach of the authors is in line with the literature according to which prior information about the material should be used as a constraint during the non-unique retrieving process from real-valued absorption coefficients to complex-valued impedances (Mondet *et al.*, 2020). In detail, α_{GA} uncertainties are expected for the macro-layers corresponding to theatre boxes (D'Orazio *et al.*, 2019; Prodi *et al.*, 2015; Sato *et al.*, 2012), thin wooden parts with air cavity (Cox and d'Antonio, 2016; Vorländer, 2020), and seat rows (D'Orazio *et al.*, 2020b; Hidaka and Beranek, 2000).

Figure 5 shows the mean differences in percentage between FDTD and GA datasets at the end of the FDTD calibrations: $\Delta\alpha$ values refer to the difference $\alpha_{\mathrm{GA}} - \alpha_{\mathrm{FDTD}}$ where α_{GA} are the energy parameters actually assigned to the surfaces and α_{FDTD} have been re-converted from the acoustic admittances actually used in the simulation (see also Table IV

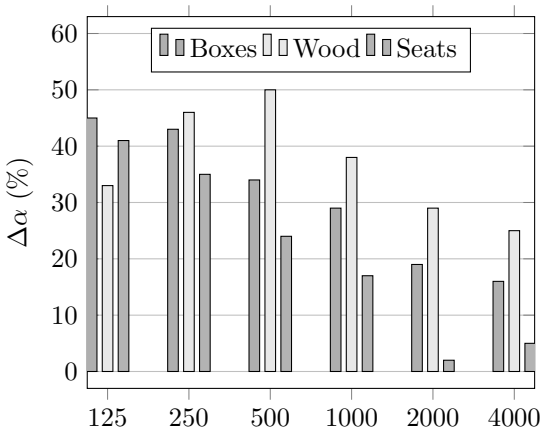

FIG. 5. (Color online) Mean values of percentage differences between FDTD and GA datasets employed as input data for the calibration processes. $\Delta\alpha = \alpha_{\mathrm{GA}} - \alpha_{\mathrm{FDTD}}$ where α_{GA} are the energy parameters actually assigned to the surfaces and α_{FDTD} have been re-converted from the acoustic admittances actually used in the simulation. Whilst "wood" and "seats" values refer to the halls A, B, C, D; "boxes" values refer only to halls A, B, C, since D has balconies instead of theatre boxes.

for a full overview). Values related to theatre "boxes" are with reference to halls A, B, C, while values related to "wood" and "seats" are with reference to halls A, B, C, D. Figure 5 shows that α_{FDTD} values are actually lower than α_{GA} values for those groups of layers, with more accentuated differences at low frequencies. It is worth noting that a decrease up to 50 % may be required from α_{GA} values to obtain α_{FDTD} values. The mean difference in percentage is 39% in the octave bands centered on 125 Hz, 250 Hz, 500 Hz, whereas it drops to 20% for the upper octave bands assessed. The discrepancies of input datasets at low frequencies are consistent with literature (Mondet *et al.*, 2020; Sakamoto *et al.*, 2008),

even though the present work involves different methodological approaches and out of the ordinary acoustic scenarios.

Since in room acoustic simulations the common datasets of surface materials typically involve energy parameters, the outcomes presented in this section could be useful as a starting point for a potential decrease of α_{GA} values for retrieving processes to obtain complex impedances. It may be concluded that the experience of the user and the knowledge of acoustic macro-effects of the rooms under study are still important in the management of input data (Pilch, 2020).

V. RESULTS AND DISCUSSIONS

The present section illustrates the actual ability of the FDTD code to detect particular acoustic features in distinct audience areas (Jeon *et al.*, 2008). The first set of outcomes shows the Bayesian multi-decay analysis carried out on the simulated impulse responses. The second part of the results presents the comparison of measured, GA and FDTD spectral contents for particularly demanding scenarios: the lack of source-receiver direct sightline and the overhang effects.

A. Multi-slope decay in coupled-volume halls

Coupled-volume geometries significantly affect the decay-curve shape. This is mainly caused by spatial dependent factors, deriving from non-diffuse transfer of energy between the subvolumes and the strong influence of relative source-receiver position (Summers *et al.*, 2004). In opera houses the decays generally show the so-called "cliff-type" characteristics,

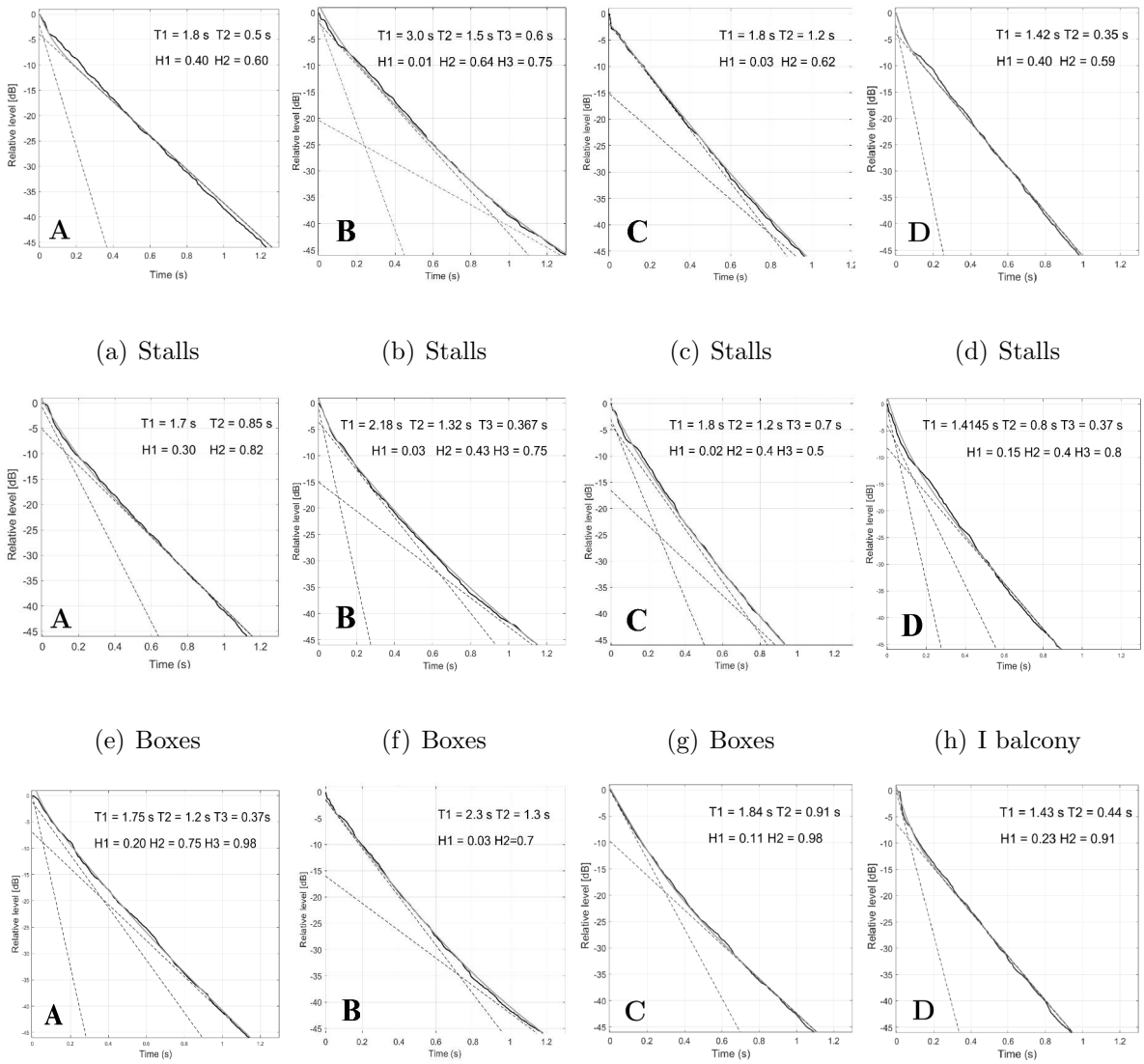

(a) Stalls (b) Stalls (c) Stalls (d) Stalls

(e) Boxes (f) Boxes (g) Boxes (h) I balcony

(i) Gallery (j) Gallery (k) Gallery (l) II balcony

FIG. 6. (Color online) Multi-decay analysis of FDTD simulated IRs (Xiang *et al.*, 2011) at 1000 Hz in all the opera houses (A, B, C, D). The position of the sound source is at the centre of the stage (S2 in Figure 2) and each receiver's position belongs to a specific audience area. The black solid lines are the Schroeder decays derived from the simulated IRs, the dashed lines are the Bayesian decay components, the orange line is the resulting decay model curve. See text for the explanation of the quantities.

with EDT values smaller than T_{30} values (Barron, 1995c). Multi-decay analysis performed on the impulse responses generally allows these effects caused by coupled-volumes to be revealed (Xiang *et al.*, 2011).

In the present section the ability of FDTD to detect those complex acoustic phenomena depending on the location of the listeners is investigated. Main results are provided in Figure 6 in terms of Bayesian analysis applied to the simulated IRs at 1000 Hz corresponding to three different source-receiver pairs in each hall. In this kind of analysis, the sound source is always located at the centre stage position (S2 points in Figure 2) and each receiver belongs to a distinct audience area (stalls, boxes and gallery in A, B, C; stalls, I balcony and II balcony in D). The decay parameters provided at top right of each subfigure should be considered with reference to the following expression:

$$H_S(\mathbf{H}, \mathbf{T}, t_k) = H_0(t_K - t_k) + \sum_{s=1}^{S} H_s e^{-13.8 t_k / T_s} \tag{10}$$

where H_S are the Schroeder decay functions, $\mathbf{T} = \mathrm{T}_1, \mathrm{T}_2, \ldots \mathrm{T}_S$ and $\mathbf{H} = \mathrm{H}_1, \mathrm{H}_2, \ldots \mathrm{H}_S$ are the decay parameters (Xiang *et al.*, 2011), S is the number of exponential decay terms that maximize the likelihood, K is a large number of data points ($1 \leq t_k \leq K$), and the linear term $H_0(t_K - t_k)$ is the background noise (not provided in Fig. 6). Figure 6 shows at least two slopes ($S = 2$) in all the source-receiver pairs because the volumes divided by the proscenium arch, i.e. the fly tower and the main hall, correspond to the two main sound energy contributions (D'Orazio *et al.*, 2020a; Garai *et al.*, 2016). The number of slopes may increase up to 3 when the receiver is in the theatre boxes (Figs. 6(f), 6(g)) or in the overhung seats (Fig. 6(h)), showing a considerably lower EDT compared to T_{30}. As EDT is more related to perceived reverberance, this effect is in line with the typical acoustic

perception in the boxes (Prodi *et al.*, 2015) and in the balconies (Barron, 1995a). In fact, the first steep Bayesian decay component accounts for the weak early reflections caused by the sound absorbing materials that are closer to the receiver (Sato *et al.*, 2012). However, Figure 6(e) shows only two slopes, meaning that in the opera house with the highest value of coupling factor ($k_c = 0.35$ in hall A) the main hall and the fly tower act more as a single acoustic volume from the point of view of a listener in the boxes (D'Orazio *et al.*, 2020b). The number of the slopes tend to decrease in the stalls due to the presence of reflective sidewalls all around the seats (Garai *et al.*, 2015). With reference to Table I, it is important to note that hall A and hall B are affected by stronger coupling effects between the fly tower and the main hall ($k_c > 0.20$) compared to hall C and hall D ($k_c < 0.20$) (D'Orazio *et al.*, 2020b). In fact, three slopes are also detected for the receiver in the gallery in hall A (Fig. 6(i)) and for the receiver in the stalls in hall B (Fig. 6(b)), confirming the accentuated coupling effects of these two opera houses compared, respectively, to Figs. 6(j), 6(k), 6(l) and Figs. 6(a), 6(c), 6(d).

The FDTD model was here validated as an accurate simulation approach able to detect complex coupling effects in different audience areas. In the present section these particular acoustic phenomena are assessed from an energetic-statistic point of view, i.e. Bayesian multi-slope analysis, whereas in the following section they are evaluated in terms of spectral information.

B. Spectral content in challenging scenarios

With the goal to further investigate the performance of FDTD simulations, the frequency response of specific source-receiver pairs is here reported (Hornikx *et al.*, 2015a; Soares *et al.*, 2022; Wang *et al.*, 2019). The spectral analysis of measured and simulated impulse responses is provided to assess the ability of the FDTD simulation framework to return reliable results even in particular acoustic scenarios (Aretz *et al.*, 2009). Figure 7 shows the spectral contribution in two specific situations occuring in hall A and hall D: measured (black), FDTD simulated (orange) frequency responses are shown along with the corresponding condition simulated through GA techniques (green). Each frequency response has been third octave band filtered and reported up to 4000 Hz. All the frequency responses involved have been properly shifted to facilitate the comparison. Figure 7(a) refers to a configuration with no direct sightline in hall A: the sound source in the orchestra pit and the listener in the stalls. Such a source-receiver pair represents a demanding task for any simulation approach because most of the energy contribution at the receiver comes from the scattered sound energy from the edges of the orchestra pit (Barron, 2009; Meyer, 2009). At low frequencies it is possible to notice a considerable gap between the two simulation approaches (more than 10 dB at 125 Hz and 250 Hz). The handling of wave phenomena, such as the edge diffraction caused by the orchestra rail, accentuates the inherent and unavoidable discrepancies between wave-based and ray-based methods (Savioja and Svensson, 2015). Compared to the measures, in Figure 7(a) the overall average Normalized Root Mean Square Error (NRMSE) is equal to 8.6 for GA and 2.8 for FDTD. Figure 7(b) provides the results for the following

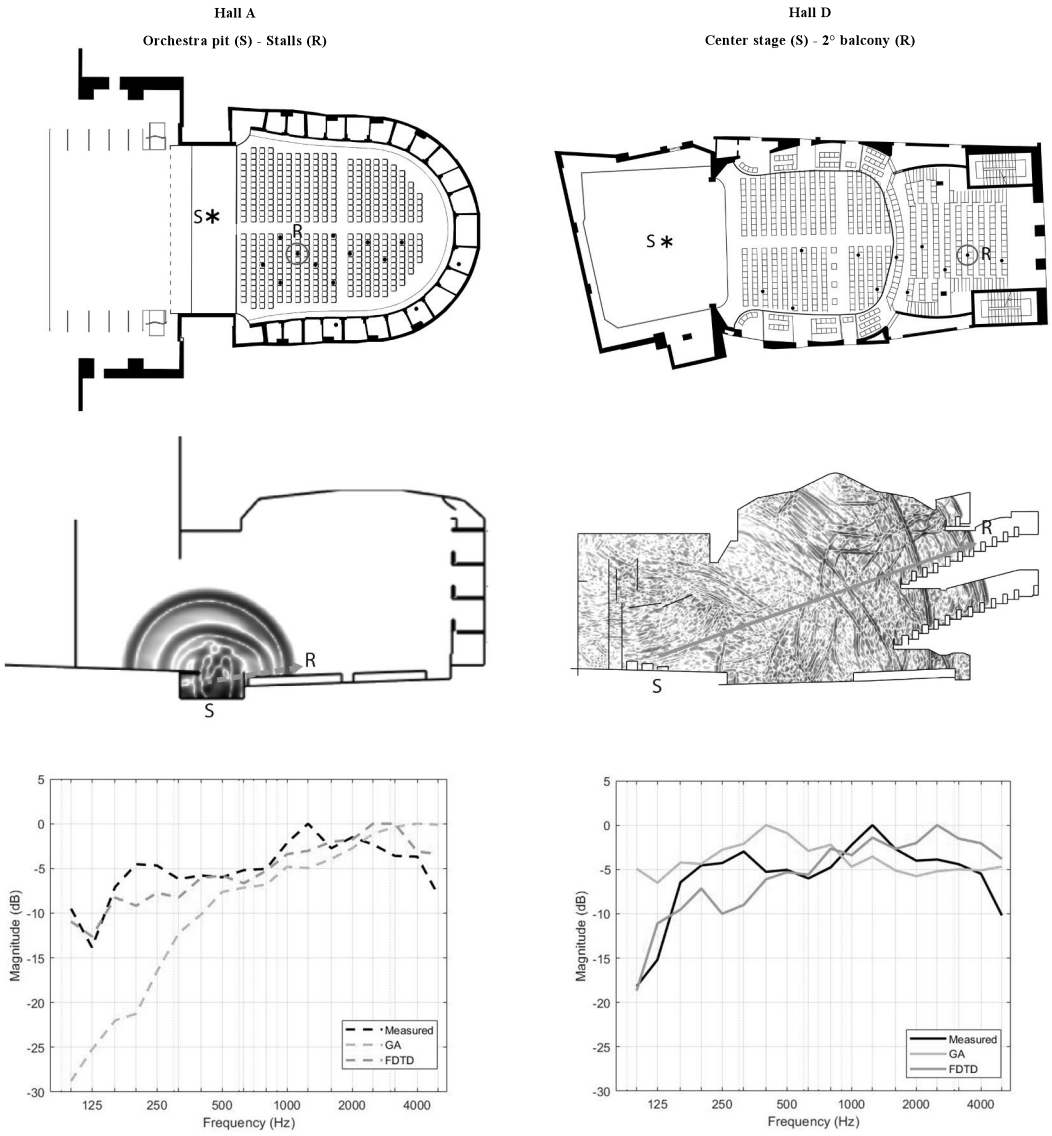

(a) Orchestra pit (S) - Stalls (R) (b) Stage (S) - II balcony (R)

FIG. 7. (Color online) Spectral content of IRs corresponding to two challenging acoustic scenarios: on the left (hall A) no direct sightline (dashed line) between the sound source (S) in the orchestra pit and the receiver (R) in the stalls; on the right (hall D) balcony overhangs with the sound source (S) on the stage and the receiver (R) in the II balcony. Comparison among frequency responses derived from measured, FDTD simulated and GA simulated IRs is provided in third octave bands.

configuration in hall D: the sound source at the centre of the stage and the listener in the overhangs of the second balcony. As hall D is a performance space with weaker coupling effects, acoustic simulations are generally expected to provide more accurate results in terms of acoustical parameters for each audience area (Summers *et al.*, 2004). In fact, it is possible to observe that the similarity between the spectral information of the measured IRs and the simulated IRs with FDTD and GA methods in Figure 7(b) is generally higher than Figure 7(a) due to the direct sightline between the sound source and the receiver (NRMSE$<$ 5 for both the methods). However, some discrepancies among the frequency responses are still present. For instance, the gap between measured and FDTD at 250 Hz reflects the difficulty of computing the unpredictable level variations in overhung seats at low frequencies, which are strongly affected by grazing incidence (Barron, 1995b). Concerning measured and GA values, greater deviations are visible at 125 Hz (more than 12 dB). In Figure 7(b) the overall average NRMSE is 4.7 for GA and 3.3 for FDTD.

In order to further check and validate the reliability of the FDTD code up to 4000 Hz, the match between the traditional IR room acoustic parameters derived from measurements and from FDTD simulations are provided for the same two source-receiver pairs. Figure 8 shows the comparison between measured (black markers) and FDTD simulated (white markers) T_{30}, EDT, C_{80}, T_{S} from 125 Hz to 4000 Hz: 75% of the differences between measured and simulated values lie within the tolerance ranges (error bars) chosen for each room criterion.

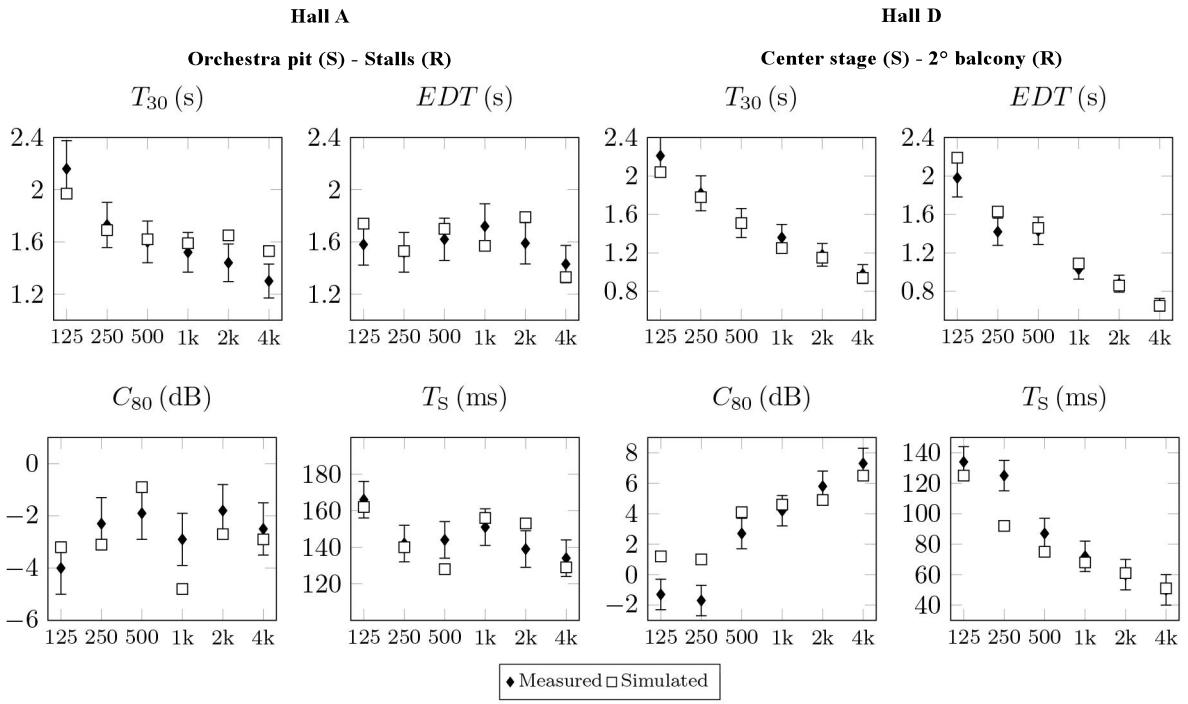

FIG. 8. Measured and FDTD simulated T_{30}, EDT, C_{80}, T_S values for the same source-receiver pairs assessed in Figure 7. The tolerance ranges selected for each parameter are also shown: 10 % for T_{30}, 10 % for EDT; 1 dB for C_{80}, 10 ms for T_S.

CONCLUSIONS

In conclusion, the main concerns about using FDTD methods in non-trivial large environments have been primarily caused by high computational cost and the implementation of frequency-dependent wall impedances. Such issues, that represented significant obstacles up to the most recent decades, have been increasingly overcome in the last years. In the present work, current opportunities in FDTD large-scale room acoustics applications have been exploited, with a special focus on the input data assigned to the boundaries and the simulation of acoustic coupling phenomena.

The FDTD model chosen for this study was tested in four different large-scale coupled-volume halls for wider frequency ranges compared to the usual wave-based applications. The FDTD calibration of the 3D virtual models was developed keeping the parallel standard GA procedure by way of comparison. At the end of the calibration processes, the analysis of input datasets used in the two simulation approaches has been provided in term of differences between α_{GA} and the equivalent α_{FDTD} derived from complex-valued impedances actually employed in FDTD calibrations. The outcomes highlight a significant overestimation of α_{GA} compared to α_{FDTD} with accentuated discrepancies at low frequencies, in line with previous findings.

Moreover, the accuracy of the results and the reliability of the overall process have been validated by means of Bayesian multi-decay analysis and spectral contents' assessment for challenging source-receiver pairs. The former insight confirms the ability of the wave-based approach to detect specific acoustic coupling phenomena, such as the presence of 3 decay components in theatre boxes. These outcomes are consistent with the engaged literature on opera houses and the typical acoustic traits in each audience area. The latter analysis proves the spectral information to be reasonably well modeled by the FDTD model up to 4 kHz, even in the case of source-receiver with no direct sightline or in case of strong grazing incidence in overhung seats in the balconies. Materials employed for calibrating the coupled-volume virtual opera houses - including 3D models, measurements' results, boundary conditions - are freely available in online repositories (Fratoni, a,b).

ACKNOWLEDGMENTS

The authors would like to thank Anna Rovigatti for having patiently helped to calibrate GA models.

	Material	125 Hz	250 Hz	500 Hz	1000 Hz	2000 Hz	4000 Hz
	A						
Both	Marble	0.02	0.02	0.03	0.03	0.04	0.05
	Plaster	0.09	0.09	0.09	0.10	0.10	0.10
	Carpet	0.04	0.05	0.06	0.08	0.16	0.20
	Curtains	0.10	0.16	0.50	0.65	0.73	0.73
	Stage house	0.25	0.25	0.25	0.25	0.20	0.20
	Stage grid	0.35	0.45	0.50	0.65	0.65	0.65
	Seats	0.35	0.45	0.55	0.60	0.60	0.60
FDTD	Boxes	0.08	0.12	0.14	0.15	0.15	0.15
	Wooden stage	0.20	0.15	0.10	0.10	0.10	0.10
GA	Boxes	0.16	0.25	0.29	0.29	0.30	0.30
	Wooden stage	0.30	0.28	0.20	0.16	0.14	0.05
	B						
	Marble	0.01	0.01	0.01	0.02	0.02	0.02

	Plaster	0.03	0.03	0.04	0.04	0.04	0.04
	Wooden linings	0.22	0.12	0.10	0.08	0.06	0.07
	Curtains	0.05	0.10	0.11	0.18	0.30	0.35
	Stage house	0.05	0.03	0.03	0.03	0.03	0.03
	Stage grid	0.25	0.35	0.55	0.55	0.55	0.55
	Wooden stage	0.18	0.12	0.10	0.09	0.08	0.07
FDTD	Boxes	0.15	0.14	0.14	0.12	0.16	0.18
	Seats	0.20	0.30	0.40	0.50	0.52	0.58
GA	Boxes	0.22	0.30	0.30	0.25	0.22	0.22
	Seats	0.40	0.50	0.58	0.61	0.58	0.58
	C						
	Marble	0.01	0.01	0.02	0.02	0.02	0.02
	Plaster	0.02	0.02	0.03	0.03	0.03	0.03
	Curtains	0.15	0.35	0.55	0.77	0.70	0.60
	Stage house	0.12	0.14	0.15	0.15	0.16	0.16
	Stage grid	0.15	0.15	0.25	0.40	0.55	0.55
	Wooden ceiling	0.18	0.12	0.10	0.09	0.08	0.07

FDTD	Boxes	0.09	0.18	0.30	0.35	0.38	0.38
	Seats	0.20	0.38	0.55	0.65	0.80	0.75
GA	Boxes	0.20	0.22	0.30	0.40	0.40	0.40
	Seats	0.40	0.55	0.70	0.80	0.80	0.70
	D						
	Marble	0.01	0.01	0.02	0.02	0.03	0.03
	Plaster	0.01	0.03	0.03	0.04	0.06	0.06
	Curtains	0.20	0.35	0.35	0.45	0.50	0.50
	Stage house	0.12	0.15	0.15	0.18	0.18	0.18
	Stage grid	0.15	0.15	0.25	0.40	0.50	0.50
	Carpet	0.04	0.07	0.15	0.20	0.25	0.30
FDTD	Seats (stalls)	0.35	0.32	0.40	0.50	0.60	0.65
	Seats (balconies)	0.48	0.60	0.50	0.60	0.52	0.62
GA	Seats (stalls)	0.48	0.50	0.50	0.58	0.58	0.60
	Seats (balconies)	0.52	0.60	0.78	0.88	0.70	0.65

TABLE IV: Main material properties employed in the simulation of hall A, B, C, D. Energy parameters have been fitted through RLC circuit analogy. See text for details.

Alvarez-Morales, L., and Martellotta, F. (**2015**). "A geometrical acoustic simulation of the effect of occupancy and source position in historical churches," Applied Acoustics **91**, 47–58.

Aretz, M., Nöthen, R., Vorländer, M., and Schröder, D. (**2009**). "Combined broadband impulse responses using fem and hybrid ray-based methods," in *EAA Symposium on Auralization*, pp. 15–17.

Barron, M. (**1995**a). "Balcony overhangs in concert auditoria," The Journal of the Acoustical Society of America **98**(5), 2580–2589.

Barron, M. (**1995**b). "Bass sound in concert auditoria," The Journal of the Acoustical Society of America **97**(2), 1088–1098.

Barron, M. (**1995**c). "Interpretation of early decay times in concert auditoria," Acta Acustica united with Acustica **81**(4), 320–331.

Barron, M. (**2009**). *Auditorium acoustics and architectural design* (Routledge).

Bilbao, S., Hamilton, B., Botts, J., and Savioja, L. (**2015**). "Finite volume time domain room acoustics simulation under general impedance boundary conditions," IEEE/ACM Transactions on Audio, Speech, and Language Processing **24**(1), 161–173.

Bilbao, S. D. (**2009**). *Numerical sound synthesis* (Wiley Online Library).

Bork, I. (**2005**). "Report on the 3rd round robin on room acoustical computer simulation–part ii: Calculations," Acta Acustica united with Acustica **91**(4), 753–763.

Botteldooren, D. (**1995**). "Finite-difference time-domain simulation of low-frequency room acoustic problems," The Journal of the Acoustical Society of America **98**(6), 3302–3308.

Brinkmann, F., Aspöck, L., Ackermann, D., Lepa, S., Vorländer, M., and Weinzierl, S. (**2019**). "A round robin on room acoustical simulation and auralization," The Journal of the Acoustical Society of America **145**(4), 2746–2760.

Christensen, C. L. (**1998**). "Odeon room acoustics program version 3.1-user manual: Industrial, auditorium and combined editions," .

Courant, R., Friedrichs, K., and Lewy, H. (**1928**). "Über die partiellen differenzengleichungen der mathematischen physik," Mathematische annalen **100**(1), 32–74.

Cox, T., and d'Antonio, P. (**2016**). *Acoustic absorbers and diffusers: theory, design and application* (Crc Press).

Cremer, L., and Müller, H. A. (**1978**). *Die wissenschaftlichen grundlagen der raumakustik* (Hirzel Stuttgart).

D'Orazio, D., De Cesaris, S., Guidorzi, P., Barbaresi, L., Garai, M., and Magalotti, R. (**2016**). "Room acoustic measurements using a high spl dodecahedron," in *Audio Engineering Society Convention 140*, Audio Engineering Society.

D'Orazio, D., Fratoni, G., and Garai, M. (**2020**a). "Enhancing the strength of symphonic orchestra in an opera house," Applied Acoustics **170**, 107532.

D'Orazio, D., Fratoni, G., Rovigatti, A., and Garai, M. (**2020**b). "A virtual orchestra to qualify the acoustics of historical opera houses," Building Acoustics 1351010X20912501.

D'Orazio, D., Rovigatti, A., and Garai, M. (**2019**). "The proscenium of opera houses as a disappeared intangible heritage: a virtual reconstruction of the 1840s original design of the

459 alighieri theatre in ravenna," in *Acoustics*, Multidisciplinary Digital Publishing Institute,
460 Vol. 1, pp. 694–710.

461 Fratoni, G. (a). "Materials for calibrating coupled-volume virtual opera houses through
462 acoustic simulations," doi.org/10.17632/kgj4h7ddcd.

463 Fratoni, G. (b). "Materials for calibrating four complex virtual environments through acous-
464 tic simulations," doi.org/10.17632/y7xnv6xg5s.

465 Garai, M., De Cesaris, S., Morandi, F., and D'Orazio, D. (**2016**). "Sound energy distribution
466 in italian opera houses," in *Proceedings of Meetings on Acoustics 22ICA*, Acoustical Society
467 of America, Vol. 28, p. 015019.

468 Garai, M., Morandi, F., D'Orazio, D., De Cesaris, S., and Loreti, L. (**2015**). "Acoustic
469 measurements in eleven italian opera houses: Correlations between room criteria and con-
470 siderations on the local evolution of a typology," Building and Environment **94**, 900–912.

471 Hamilton, B. (**2016**). "Finite difference and finite volume methods for wave-based modelling
472 of room acoustics. ph.d. dissertation. university of edinburgh, uk.," Ph.D. thesis.

473 Hamilton, B. (**2021**). "Adding air attenuation to simulated room impulse responses: A
474 modal approach," arXiv preprint arXiv:2107.11871 .

475 Hamilton, B., Webb, C., Fletcher, N., and Bilbao, S. (**2016**). "Finite difference room acous-
476 tics simulation with general impedance boundaries and viscothermal losses in air: Parallel
477 implementation on multiple gpus," in *Proc. Int. Symp. Musical Room Acoust.*

478 Hamilton, B., and Webb, C. J. (**2013**). "Room acoustics modelling using gpu-accelerated
479 finite difference and finite volume methods on a face-centered cubic grid," Proc. Digital
480 Audio Effects (DAFx), Maynooth, Ireland 336–343.

481 Hidaka, T., and Beranek, L. L. (**2000**). "Objective and subjective evaluations of twenty-
482 three opera houses in europe, japan, and the americas," The Journal of the Acoustical
483 Society of America **107**(1), 368–383.

484 Hornikx, M., Hak, C., and Wenmaekers, R. (**2015**a). "Acoustic modelling of sports halls,
485 two case studies," Journal of Building Performance Simulation **8**(1), 26–38.

486 Hornikx, M., Kaltenbacher, M., and Marburg, S. (**2015**b). "A platform for benchmark cases
487 in computational acoustics," Acta Acustica United With Acustica **101**(4), 811–820.

488 Jeon, J. Y., Kim, Y. H., Cabrera, D., and Bassett, J. (**2008**). "The effect of visual and
489 auditory cues on seat preference in an opera theater," The Journal of the Acoustical
490 Society of America **123**(6), 4272–4282.

491 Jeong, C.-H. (**2009**). "A correction of random incidence absorption coefficients for the an-
492 gular distribution of acoustic energy under measurement conditions," The Journal of the
493 Acoustical Society of America **125**(4), 2064–2071.

494 Jeong, C.-H. (**2012**). "Absorption and impedance boundary conditions for phased
495 geometrical-acoustics methods," The Journal of the Acoustical Society of America **132**(4),
496 2347–2358.

497 Jeong, C.-H., Ih, J.-G., and Rindel, J. H. (**2008**). "An approximate treatment of reflection
498 coefficient in the phased beam tracing method for the simulation of enclosed sound fields
499 at medium frequencies," Applied Acoustics **69**(7), 601–613.

500 Jeong, C.-H., Marbjerg, G., and Brunskog, J. (**2016**). "Uncertainty of input data for room
501 acoustic simulations," in *Proc. of bi-annual Baltic-Nordic Acoustic Meeting*.

Kim, Y. H., Lee, H. M., Seo, C. K., and Jeon, J. Y. (**2010**). "Investigating the absorption characteristics of open ceilings in multi-purpose halls using a 1: 25 scale model," Applied acoustics **71**(5), 473–478.

Kowalczyk, K., and Van Walstijn, M. (**2010**). "Room acoustics simulation using 3-d compact explicit fdtd schemes," IEEE Transactions on Audio, Speech, and Language Processing **19**(1), 34–46.

Krokstad, A., Strom, S., and Sørsdal, S. (**1968**). "Calculating the acoustical room response by the use of a ray tracing technique," Journal of Sound and Vibration **8**(1), 118–125.

Lai, H., and Hamilton, B. (**2020**). "Computer modeling of barrel-vaulted sanctuary exhibiting flutter echo with comparison to measurements," in *Acoustics*, Multidisciplinary Digital Publishing Institute, Vol. 2, pp. 87–109.

Luizard, P., Otani, M., Botts, J., Savioja, L., and Katz, B. F. (**2013**). "Comparison of sound field measurements and predictions in coupled volumes between numerical methods and scale model measurements," in *Proceedings of Meetings on Acoustics ICA2013*, Acoustical Society of America, Vol. 19, p. 015114.

Marbjerg, G., Brunskog, J., Jeong, C.-H., and Nilsson, E. (**2015**). "Development and validation of a combined phased acoustical radiosity and image source model for predicting sound fields in rooms," The Journal of the Acoustical Society of America **138**(3), 1457–1468.

Marburg, S., and Nolte, B. (**2008**). *Computational acoustics of noise propagation in fluids: finite and boundary element methods*, **578** (Springer).

Meyer, J. (**2009**). *Acoustics and the performance of music: Manual for acousticians, audio engineers, musicians, architects and musical instrument makers* (Springer Science &

524 Business Media).

525 Mondet, B., Brunskog, J., Jeong, C.-H., and Rindel, J. H. (**2020**). "From absorption to
526 impedance: Enhancing boundary conditions in room acoustic simulations," Applied Acous-
527 tics **157**, 106884.

528 Pilch, A. (**2020**). "Optimization-based method for the calibration of geometrical acoustic
529 models," Applied Acoustics **170**, 107495.

530 Pind, F., Engsig-Karup, A. P., Jeong, C.-H., Hesthaven, J. S., Mejling, M. S., and Strømann-
531 Andersen, J. (**2019**). "Time domain room acoustic simulations using the spectral element
532 method," The Journal of the Acoustical Society of America **145**(6), 3299–3310.

533 Pompoli, R., and Prodi, N. (**2000**). "Guidelines for acoustical measurements inside historical
534 opera houses: procedures and validation," Journal of sound and vibration **232**(1), 281–301.

535 Postma, B. N., and Katz, B. F. (**2015**). "Creation and calibration method of acoustical
536 models for historic virtual reality auralizations," Virtual Reality **19**(3), 161–180.

537 Prodi, N., Pompoli, R., Martellotta, F., and Sato, S.-i. (**2015**). "Acoustics of italian histor-
538 ical opera houses," The Journal of the Acoustical Society of America **138**(2), 769–781.

539 Rindel, J. H. (**2000**). "The use of computer modeling in room acoustics," Journal of vibro-
540 engineering **3**(4), 219–224.

541 Rindel, J. H. (**2011**). "An impedance model for estimating the complex pressure reflection
542 factor," in *Forum Acusticum*, Vol. 2011.

543 Saarelma, J., and Savioja, L. (**2016**). "Audibility of dispersion error in room acoustic finite-
544 difference time-domain simulation in the presence of absorption of air," The Journal of the
545 Acoustical Society of America **140**(6), EL545–EL550.

Sakamoto, S., Nagatomo, H., Ushiyama, A., and Tachibana, H. (**2008**). "Calculation of impulse responses and acoustic parameters in a hall by the finite-difference time-domain method," Acoustical science and technology **29**(4), 256–265.

Sato, S.-i., Wang, S., Zhao, Y., Wu, S., Sun, H., Prodi, N., Visentin, C., and Pompoli, R. (**2012**). "Effects of acoustic and visual stimuli on subjective preferences for different seating positions in an italian style theater," Acta Acustica united with Acustica **98**(5), 749–759.

Savioja, L. (**2010**). "Real-time 3d finite-difference time-domain simulation of low-and mid-frequency room acoustics," in *13th Int. Conf on Digital Audio Effects*, Vol. 1, p. 75.

Savioja, L., and Svensson, U. P. (**2015**). "Overview of geometrical room acoustic modeling techniques," The Journal of the Acoustical Society of America **138**(2), 708–730.

Siltanen, S., Lokki, T., Savioja, L., and Lynge Christensen, C. (**2008**). "Geometry reduction in room acoustics modeling," Acta Acustica united with Acustica **94**(3), 410–418.

Soares, M. C., Carneiro, E. B., Tenenbaum, R. A., and Mareze, P. H. (**2022**). "Low-frequency room acoustical simulation of a small room with bem and complex-valued surface impedances," Applied Acoustics **188**, 108570.

Southern, A., Siltanen, S., Murphy, D. T., and Savioja, L. (**2013**). "Room impulse response synthesis and validation using a hybrid acoustic model," IEEE Transactions on Audio, Speech, and Language Processing **21**(9), 1940–1952.

Strikwerda, J. (**1989**). "Finite difference schemes partial differential equations. wadsworth & brooks/cole" .

567 Summers, J. E., Torres, R. R., and Shimizu, Y. (**2004**). "Statistical-acoustics models of
568 energy decay in systems of coupled rooms and their relation to geometrical acoustics,"
569 The Journal of the Acoustical Society of America **116**(2), 958–969.

570 Vercammen, M. (**2019**). *On the revision of ISO 354, measurement of the sound absorption*
571 *in the reverberation room* (Universitätsbibliothek der RWTH Aachen).

572 Vorländer, M. (**2013**). "Computer simulations in room acoustics: Concepts and uncertain-
573 ties," The Journal of the Acoustical Society of America **133**(3), 1203–1213.

574 Vorländer, M. (**2020**). *Auralization* (Springer).

575 Wang, H., Sihar, I., Pagán Muñoz, R., and Hornikx, M. (**2019**). "Room acoustics modelling
576 in the time-domain with the nodal discontinuous galerkin method," The Journal of the
577 Acoustical Society of America **145**(4), 2650–2663.

578 Wareing, A., and Hodgson, M. (**2005**). "Beam-tracing model for predicting sound fields
579 in rooms with multilayer bounding surfaces," The Journal of the Acoustical Society of
580 America **118**(4), 2321–2331.

581 Webb, C. J., and Bilbao, S. (**2011**). "Computing room acoustics with cuda-3d fdtd schemes
582 with boundary losses and viscosity," in *2011 IEEE International Conference on Acoustics,*
583 *Speech and Signal Processing (ICASSP)*, IEEE, pp. 317–320.

584 Xiang, N., Goggans, P., Jasa, T., and Robinson, P. (**2011**). "Bayesian characterization
585 of multiple-slope sound energy decays in coupled-volume systems," The Journal of the
586 Acoustical Society of America **129**(2), 741–752.